Analytical Large-Signal Modeling of Inverter-based Microgrids with Koopman Operator Theory for Autonomous Control

Zixiao Ma, *Member, IEEE*, Zhaoyu Wang, *Senior Member, IEEE* and Rui Cheng, *Member, IEEE*

***Abstract*—The microgrid (MG) plays a crucial role in the energy transition, but its nonlinearity presents a significant challenge for large-signal power systems studies in the electromagnetic transient (EMT) time scale. In this paper, we develop a large-signal linear MG model that considers the detailed dynamics of the primary and zero-control levels based on the Koopman operator (KO) theory. Firstly, a set of observable functions is carefully designed to capture the nonlinear dynamics of the MG. The corresponding linear KO is then analytically derived based on these observables, resulting in the linear representation of the original nonlinear MG with observables as the new coordinate. The influence of external input on the system dynamics is also considered during the derivation, enabling control of the MG. We solve the voltage control problem using the traditional linear quadratic integrator (LQI) method to demonstrate that textbook linear control techniques can accurately control the original nonlinear MG via the developed KO-linearized MG model. Our proposed KO linearization method is generic and can be easily extended for different control objectives and MG structures using our analytical derivation procedure. We validate the effectiveness of our methodology through various case studies.**

***Index Terms*—Microgrid (MG), Electromagnetic transient (EMT), Koopman operator (KO), Large-signal modeling, Microgrid voltage control.**

I. Introduction

MICROGRIDS (MGs) are localized small-scale power systems with the integration of various distributed energy resources (DERs) such as solar panels, wind turbines, or generators to provide electricity to local consumers [1]–[5]. They are not only essential for enhancing the resilience, reliability, and efficiency of the power network, but also key to energy transition and decarbonization [6]. MGs can operate autonomously or be connected to the main grid. In grid-connected mode, the MG is mainly governed by the main grid. While in islanded mode, local controls are needed to coordinate multiple DERs.

For simplifying the controller design, MG control is usually decoupled based on different time scales [1], [2]. Primary and zero-control levels stabilize the DERs at the fastest and lowest layer. The secondary control eliminates the steady-state error caused by the droop characteristics. The tertiary control focuses on economic dispatching and operation scheduling in the slowest time scale. For the secondary control level, there are two major approaches. One assumes that the zero-control level can always guarantee stability and provide fast and accurate reference tracking performance so that its dynamic model can be reduced [7]. This approach significantly increases the scalability of secondary control and enables large-scale system analysis. However, it inevitably results in the loss of the faster electromagnetic transient (EMT) [8], [9]. Moreover, large disturbances such as data loss, outliers, time delays, etc. are possible to happen in the feedback channel or actuator and result in an inappropriate secondary control signal that finally deteriorates the stability of the MG [10]. Therefore, another approach is to design the secondary controller with consideration of detailed dynamics of primary and zero-control levels in the EMT time scale [11], [12]. Such an approach can capture faster dynamics and yield a more reliable control strategy, nonetheless, the consideration of these dynamics considerably increases the system order as well as complexifies the nonlinearity of MGs [12].

Control of inverter-based MGs based on a nonlinear EMT model has been widely studied over the past decade [11]–[13]. However, controller design for nonlinear systems is usually case-by-case and can hardly be generalized to cope with different situations, such as time-delays [10], uncertainties [14], [15], constraints [16], etc. Thus, some studies sort to small-signal MG models based on linearization around an equilibrium point [8], [9]. With these models, one can use spectral tools to easily analyze the linear dynamics of MGs and adopt textbook linear control techniques to achieve various control objectives [17]. However, the results obtained with small-signal models are only valid within a neighborhood around the selected equilibrium.

Recently, the Koopman operator (KO) prevails as an effective linearization method that can accurately capture large-signal nonlinear dynamics. The essential idea is that a nonlinear dynamical system can be represented by an infinite-dimensional *linear* operator on a Hilbert space of vector-valued observable functions of system states [18]. The existing KO identification approaches can be classified into numerical (data-driven) and analytical (model-based) ones [19]. In *numerical* methods, a finite set of observable functions will be firstly designed based on the knowledge of dynamical system nonlinearity. Then, the KO will be identified using the system state's measurement data pairs of snapshots as it evolves in time. Representative methods include dynamic

This work was supported in part by the U.S. Department of Energy Wind Energy Technologies Office under Grant DE-EE0008956, and in part by the National Science Foundation under ECCS 1929975 and SBE 2228620. (*Corresponding author: Zhaoyu Wang*)

Z. Ma, Z. Wang and R. Cheng are with the Department of Electrical and Computer Engineering, Iowa State University, Ames, IA 50011, USA (email: zma@iastate.edu; wzy@iastate.edu; ruicheng@iastate.edu).

mode decomposition (DMD) [20], [21] and its extensions, such as extended DMD (EDMD) [22], and extended DMD with control (EDMDc) [23], etc. Especially from the MG control perspective, the KO is applied to the secondary control problem of MG in [24], [25]. Five observable functions are initiated and the KO is estimated by the EDMDc method with the assumption that the droop gains are known by the secondary controller. The assumption on the knowledge of local controllers is further relaxed and an enhanced observer Kalman filter to optimally identify the Koopman operator is proposed in [26]. The proposed approaches well fit the studied two-dimensional state-space model, nonetheless, they cannot capture the faster dynamics in the EMT time scale since the zero-control level is not considered. There are two major challenges to extending such numerical methods to the MGs modeled with EMT: firstly, to capture the EMT dynamics, model-free data-driven methods require measurements of the lower control levels, nonetheless, these measurements are usually not available due to limited meters; secondly, the dynamics of the lower control level significantly lift the observable space, such that an *exponentially increased volume of data pairs* are required for the numerical methods to produce an accurate estimation of the KO.

Another way to apply KO theory to *high-order nonlinear systems* is to use *analytical* methods that rely on the choice of observable functions [27]. If the observable functions are chosen perfectly, the nonlinear system can be represented in the lifted Hilbert space without any error. However, this is usually unachievable for most practical systems. A common strategy is to start with a set of observable functions and then expand them until the error between the nonlinear model and the KO linear model is sufficiently small [28]. Analytical methods provide an explicit linear model that does not need to be re-identified for different system settings as in numerical methods. However, deriving the KO analytically usually depends on the specific nonlinear dynamics of a practical system. For instance, [28] studied a nonlinear attitude control problem using the KO and selected the observables as the first nth-order derivatives of attitude dynamics. In [29], the KO was used to generate approximate analytical solutions for the motion of a satellite orbiting a non-spherical celestial body with zonal harmonics. It showed that the KO could capture any order of zonal harmonics without changing the methodology. To our best knowledge, no existing study has applied an analytical KO derivation method to MG control problems.

This paper proposes an analytical KO-based large-signal model linearization approach for inverter-dominated islanded MGs. The approach considers the detailed dynamics of primary and zero-control levels in the EMT time scale. To capture the nonlinear dynamics of the MG, we design a set of observables meticulously. Then, a KO is derived analytically to represent the original nonlinear MG linearly with these observables as the new coordinate. To demonstrate that standard linear techniques are conveniently applicable, we solve the voltage control problem using the conventional linear quadratic integrator (LQI) method as an example. The main contributions of this paper are summarized as follows:

- A novel linear EMT MG model considering dynamics of primary and zero-control levels is proposed based on the KO theory that represents the nonlinear MG linearly with a finite set of tailored observable functions.
- Analytically derived KO is utilized to capture the nonlinear dynamics of the MG, thereby avoiding the need for huge data sets required by numerical approaches for high-dimensional complex nonlinear systems. Furthermore, the proposed KO-based model can be smoothly embedded into sophisticated linear control schemes.
- The proposed analytical KO-based model linearization methodology is generic and can be extended to other MGs with different control structures and topologies.

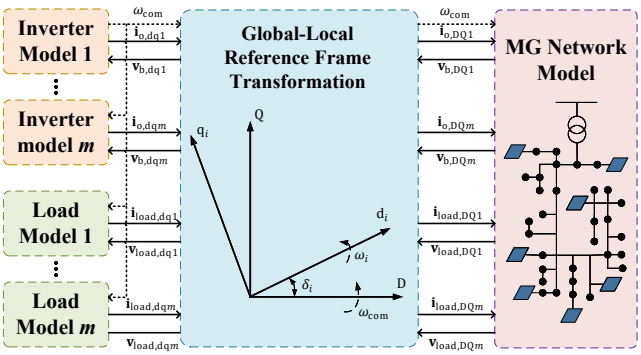

(a) Schematic of the overall MG modeling.

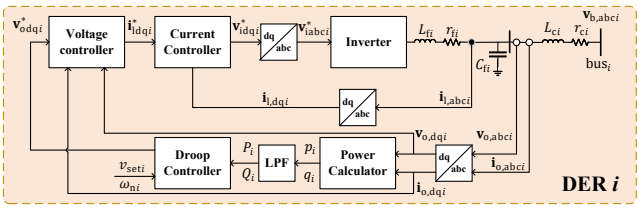

(b) Block diagram of the ith inverter.

Fig. 1. Overall diagram of a nonlinear MG system model.

II. Preliminaries

This section introduces a widely-used nonlinear MG model that forms the foundation for deriving the KO-linearized model in Section III. Additionally, the KO theory is briefly presented, with a focus on external control inputs that facilitate the use of linear control techniques.

A. MG modeling

This section introduces the detailed nonlinear mathematical model of an MG based on [8]. Figure 1 shows the schematic of the overall MG model that is operating in the islanded mode. The mathematical models are derived for each component of the MG in the following subsections.

1) Power Calculation and Droop Control: The active and reactive power produced by the system can be determined by analyzing the transformed output voltage, v_{odq}, and current, i_{odq}. To obtain the filtered instantaneous powers, a low-pass filter with a corner frequency of ω_{c} can be utilized, which yields the following results:

$$\dot{P}_i = -P_i\omega_{ci} + \omega_{ci}\left(v_{\mathrm{od}i}i_{\mathrm{od}i} + v_{\mathrm{oq}i}i_{\mathrm{oq}i}\right), \tag{1a}$$

$$\dot{Q}_i = -Q_i\omega_{ci} + \omega_{ci}\left(v_{\mathrm{oq}i}i_{\mathrm{od}i} - v_{\mathrm{od}i}i_{\mathrm{oq}i}\right). \tag{1b}$$

When operating in islanded mode, a DER lacks reference inputs from the main grid, necessitating the use of droop controllers to generate its own voltage and frequency references. The process can be achieved through the following steps:

$$\omega_i = \omega_{\rm n} - D_{{\rm P}i} P_i, \tag{2a}$$
$$v^*_{{\rm od}i} = v_{{\rm set}i} - D_{{\rm Q}i} Q_i, \tag{2b}$$
$$v^*_{{\rm oq}i} = 0. \tag{2c}$$

where $\omega_{\rm n}$ and $v_{{\rm set}i}$ are nominal frequency and voltage setpoints, respectively. The detailed determination of droop gains $D_{{\rm P}i}$ and $D_{{\rm Q}i}$ can be found in [8], [12].

2) Voltage and Current Controllers: The DER output voltages and inductor currents are usually controlled via the standard proportional–integral (PI) method at the zero level. As shown below, the voltage controllers are designed to regulate the DER output voltages to their references which are generated by the droop control at the primary level:

$$\dot{\phi}_{{\rm d}i} = v^*_{{\rm od}i} - v_{{\rm od}i}, \tag{3a}$$
$$i^*_{{\rm ld}i} = K_{{\rm iv}i}\phi_{{\rm d}i} + K_{{\rm pv}i}\dot{\phi}_{{\rm d}i} + F_i i_{\rm od} - \omega_n C_{{\rm f}i} v_{\rm oq}, \tag{3b}$$
$$\dot{\phi}_{{\rm q}i} = v^*_{{\rm oq}i} - v_{{\rm oq}i}, \tag{3c}$$
$$i^*_{{\rm lq}i} = K_{{\rm iv}i}\phi_{{\rm q}i} + K_{{\rm pv}i}\dot{\phi}_{{\rm q}i} + F_i i_{\rm oq} + \omega_n C_{{\rm f}i} v_{\rm od}. \tag{3d}$$

The commanded voltage reference, $v^*_{{\rm ldq}i}$, is generated by the current controllers through the computation of the error between the reference inductor currents, $i^*_{{\rm ldq}i}$, and corresponding feedback measurements, $i_{{\rm ldq}i}$:

$$\dot{\gamma}_{{\rm d}i} = i^*_{{\rm ld}i} - i_{{\rm ld}i}, \tag{4a}$$
$$v^*_{{\rm id}i} = -\omega_{\rm n} L_{{\rm f}i} i_{{\rm lq}i} + K_{{\rm ic}i}\gamma_{{\rm d}i} + K_{{\rm pc}i}\dot{\gamma}_{{\rm d}i}, \tag{4b}$$
$$\dot{\gamma}_{{\rm q}i} = i^*_{{\rm lq}i} - i_{{\rm lq}i}, \tag{4c}$$
$$v^*_{{\rm iq}i} = \omega_{\rm n} L_{{\rm f}i} i_{{\rm ld}i} + K_{{\rm ic}i}\gamma_{{\rm q}i} + K_{{\rm pc}i}\dot{\gamma}_{{\rm q}i}. \tag{4d}$$

3) LC Filters and Coupling Inductors: By assuming that the inverter produces the demanded voltage, i.e., $v_{{\rm id}i} = v^*_{{\rm id}i}$, $v_{{\rm iq}i} = v^*_{{\rm iq}i}$, the dynamical models of LC filters and coupling inductors are as follows

$$\dot{i}_{{\rm ld}i} = \left(-r_{{\rm f}i} i_{{\rm ld}i} + v_{{\rm id}i} - v_{{\rm od}i}\right)/L_{{\rm f}i} + \omega_i i_{{\rm lq}i}, \tag{5a}$$
$$\dot{i}_{{\rm lq}i} = \left(-r_{{\rm f}i} i_{{\rm lq}i} + v_{{\rm iq}i} - v_{{\rm oq}i}\right)/L_{{\rm f}i} - \omega_i i_{{\rm ld}i}, \tag{5b}$$
$$\dot{v}_{{\rm od}i} = \left(i_{{\rm ld}i} - i_{{\rm od}i}\right)/C_{{\rm f}i} + \omega_i v_{{\rm oq}i}, \tag{5c}$$
$$\dot{v}_{{\rm oq}i} = \left(i_{{\rm lq}i} - i_{{\rm oq}i}\right)/C_{{\rm f}i} - \omega_i v_{{\rm od}i}. \tag{5d}$$
$$\dot{i}_{{\rm od}i} = \left(-r_{{\rm c}i} i_{{\rm od}i} + v_{{\rm od}i} - v_{{\rm bd}i}\right)/L_{{\rm c}i} + \omega_i i_{{\rm oq}i}, \tag{5e}$$
$$\dot{i}_{{\rm oq}i} = \left(-r_{{\rm c}i} i_{{\rm oq}i} + v_{{\rm oq}i} - v_{{\rm bq}i}\right)/L_{{\rm c}i} - \omega_i i_{{\rm od}i}, \tag{5f}$$

4) Transforming Local Reference Frame to Global Frame: The above mathematical model of each DER is developed in their own local $d-q$ reference frame. Suppose that the local $d-q$ reference frame of the ith DER is rotating at ω_i and the global $D-Q$ reference frame is rotating at $\omega_{\rm com}$. Then, we can connect each individual DER to the network by using the following rotation transformation:

$$\begin{bmatrix} x_{{\rm D}i} \\ x_{{\rm Q}i} \end{bmatrix} = \begin{bmatrix} \cos\delta_i & -\sin\delta_i \\ \sin\delta_i & \cos\delta_i \end{bmatrix} \begin{bmatrix} x_{{\rm d}i} \\ x_{{\rm q}i} \end{bmatrix} \tag{6}$$

where x generally represents each state variable in (1)-(5). δ_i is the difference between the global reference phase and the local one of the ith DER, which is defined as

$$\dot{\delta}_i = \omega_i - \omega_{\rm com} \tag{7}$$

For islanded MGs, the first DER is selected as the common global reference in the following derivation, i.e., $\omega_{\rm com} = \omega_1$.

5) Network Model: The network model is developed in the global reference frame. The dynamic model of the ith ($i = 1, \ldots, q$) line current between bus j and bus k is represented as follows,

$$\dot{i}_{{\rm line}i} = (v_{{\rm bD}j} - v_{{\rm bD}k} - r_{{\rm line}i} i_{{\rm line}i})/L_{{\rm line}i} + \omega_i i_{{\rm lineQ}i}, \tag{8a}$$
$$\dot{i}_{{\rm line}i} = (v_{{\rm bQ}j} - v_{{\rm bQ}k} - r_{{\rm line}i} i_{{\rm line}i})/L_{{\rm line}i} - \omega_i i_{{\rm lineD}i}. \tag{8b}$$

6) Load Model: As in [8], purely resistive loads and resisters and inductors (RL loads) are considered. The purely resistive loads directly follow Ohm's law without dynamics. While the ith ($i = 1, \ldots, p$) RL load can be modeled as,

$$\dot{i}_{{\rm loadD}i} = (v_{{\rm bD}i} - R_{{\rm load}i} i_{{\rm loadD}i})/L_{{\rm load}i} + \omega_i i_{{\rm loadQ}i}, \tag{9a}$$
$$\dot{i}_{{\rm loadQ}i} = (v_{{\rm bQ}i} - R_{{\rm load}i} i_{{\rm loadQ}i})/L_{{\rm load}i} - \omega_i i_{{\rm loadD}i}. \tag{9b}$$

The frequency is constant throughout the network, thus the dynamic equations of lines and loads can adopt ω_1 derived from the first inverter [9].

7) Virtual Resistor Method: As shown in (5), (8) and (9), the bus voltages are treated as inputs to each subsystem, such that the influences of load perturbation could not be precisely predicted [9]. To define the bus voltage, a virtual resistor is assumed between each bus and the ground. By selecting a sufficiently large resistance $r_{\rm n}$ for the virtual resistor, its impact on the system dynamics can be negligible. Then, the bus voltage connecting the inverters, loads and the network can be defined as

$$v_{{\rm bD}i} = r_{\rm n}(i_{{\rm oD}i} - i_{{\rm loadD}i} + \sum_{j=1}^{N} i_{{\rm lineD}i,j}), \tag{10a}$$
$$v_{{\rm bQ}i} = r_{\rm n}(i_{{\rm oQ}i} - i_{{\rm loadQ}i} + \sum_{j=1}^{N} i_{{\rm lineQ}i,j}) \tag{10b}$$

where N is the number of lines connected to bus i. Care should be taken on the direction of line currents in the last term of (10). We assume the current entering the bus to be positive and the current leaving the bus to be negative.

B. Compact Nonlinear Model of an MG for Voltage Control

For the ease of deriving KO for the MG system, we stack up the state variables to form a compact state space model. From the viewpoint of voltage control, an inverter-based islanded MG with m DERs, p RL loads, and q lines can be represented as follows:

$$\dot{\mathbf{x}}(t) = \mathbf{f}(\mathbf{x}(t), \mathbf{u}(t)), \tag{11}$$

where $\mathbf{x} = \Big[\mathbf{x}^\top_{\rm inv1}, \ldots, \mathbf{x}^\top_{{\rm inv}m}, \mathbf{x}^\top_{\rm line1}, \ldots, \mathbf{x}^\top_{{\rm line}q}, \mathbf{x}^\top_{\rm load1}, \ldots, \mathbf{x}^\top_{{\rm load}p}\Big]^\top$ is the state vector of inverters, lines and loads; $\mathbf{x}_{{\rm inv}i} =$

$[\delta_i, P_i, Q_i, \phi_{\mathrm{d}i}, \phi_{\mathrm{q}i}, \gamma_{\mathrm{d}i}, \gamma_{\mathrm{q}i}, i_{\mathrm{ld}i}, i_{\mathrm{lq}i}, v_{\mathrm{od}i}, v_{\mathrm{oq}i}, i_{\mathrm{od}i}, i_{\mathrm{oq}i}]^\top, i = 1, \ldots, m$, denotes the state variables of the i^{th} DER; $\mathbf{x}_{\mathrm{line}i} = [i_{\mathrm{lineD}i}, i_{\mathrm{lineQ}i}]^\top, i = 1, \ldots, q$, are the currents of the i^{th} line; $\mathbf{x}_{\mathrm{load}i} = [i_{\mathrm{loadD}i}, i_{\mathrm{loadQ}i}]^\top, i = 1, \ldots, p$, are the currents of the i^{th} load; $\mathbf{u} = [v_{\mathrm{set}1}, \ldots, v_{\mathrm{set}m}]^\top$ denotes the voltage control signal to be designed. Denoting $n = 13m + 2p + 2q$, $\mathbf{f} : \mathbb{R}^n \times \mathbb{R}^m \to \mathbb{R}^n$ is the state function describing the nonlinear system dynamics. This high-dimensional dynamic model represents the detailed transient dynamics of the whole MG in the EMT time scale, thus facilitating fast dynamical analysis and control.

C. Brief Introduction of Koopman Operator Theory

The MG system described in (11) comprehensively models the primary and zero-control levels, resulting in a high-dimensional nonlinear system. Despite the increasing importance of stability analysis and controller design for dynamical systems, the system's nonlinearity presents a significant challenge for comprehensive analysis. Traditional nonlinear control methods, in particular, exhibit low generality and require complex potential function designs. From a practical standpoint, it is crucial to develop an accurate large-signal linearized MG model that bridges existing mature linear control methods and the nonlinear MG system.

The KO theory has gained considerable attention in nonlinear control theory and application as an effective linearization method that can accurately capture large-signal nonlinear dynamics. The fundamental concept of KO theory is to represent a nonlinear system as an infinite-dimensional linear operator on a Hilbert space of vector-valued observable functions $\mathbf{g}$ of system states. Recalling the MG system model (11), where $\mathbf{x}$ and $\mathbf{u}$ evolve on smooth manifolds $\mathcal{M}$ and $\mathcal{N}$, respectively, we define the *observable vector* $\mathbf{z} = \mathbf{g}(\mathbf{x}, \mathbf{u}) : \mathcal{M} \times \mathcal{N} \to \mathbb{R}^N$. Then, with an infinite-dimensional linear operator acting on the observable functions, the system dynamics of (11) can be described linearly in this Hilbert space, i.e.,

$$\begin{aligned}\mathcal{K}\mathbf{g}(\mathbf{x}, \mathbf{u}) &= \frac{d\mathbf{g}(\mathbf{x}, \mathbf{u})}{dt} \\ &= f_1 \frac{\partial \mathbf{g}}{\partial x_1} + \cdots + f_n \frac{\partial \mathbf{g}}{\partial x_n} + \dot{u}_1 \frac{\partial \mathbf{g}}{\partial u_1} + \cdots + \dot{u}_m \frac{\partial \mathbf{g}}{\partial u_m}.\end{aligned} \tag{12}$$

where $\mathbf{x} = [x_1, \ldots, x_n]$ and $\mathbf{u} = [u_1, \ldots, u_m]$. In Eq. (12), we follow the assumption in [25] that the control signals influence the state evolution, but they are not evolving dynamically, i.e., $\dot{\mathbf{u}} = \mathbf{0}$. The above equation (12) indicates that the KO intrinsically describes the dynamical evolution of the observation of the state and input $\mathbf{g}(\mathbf{x}, \mathbf{u})$ in a linear manner as illustrated in Fig. 2. Therefore, it sheds light on analyzing the system dynamics with spectral methods and design controllers with the existing general linear control methodologies for nonlinear systems (11) in the KO-oriented linear space.

From a practical engineering perspective, it is important to note that an infinite-dimensional system is not feasible. Therefore, the key to utilizing KO theory lies in identifying an appropriate set of finite-dimensional observables and the corresponding KO that captures the primary dynamics in the Hilbert space. In the following section, we develop a KO-linearized MG model with finite-dimensional observables using an analytical approach.

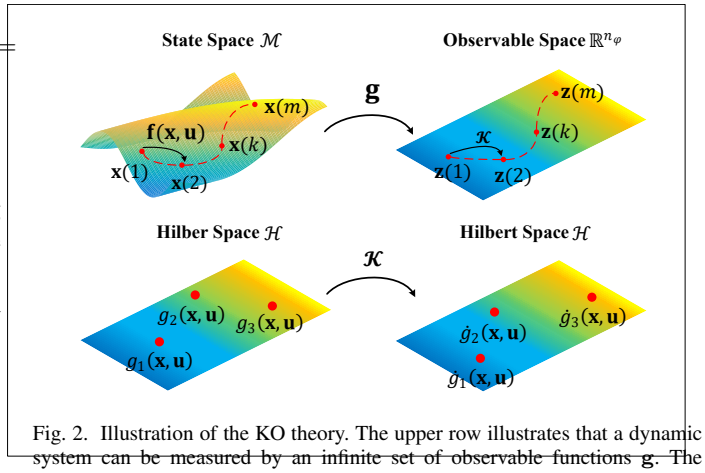

Fig. 2. Illustration of the KO theory. The upper row illustrates that a dynamic system can be measured by an infinite set of observable functions $\mathbf{g}$. The lower row explains that the KO, $\mathcal{K}$, describes the dynamical evolution of the observation of the state and input, $\mathbf{g}(\mathbf{x}, \mathbf{u})$, in a linear manner.

III. Derivation of KO-linearized MG Model

In this section, we present an analytical method to develop a KO-linearized model of the MG system (11) in the EMT time-scale, which is proposed for the first time. The derivation process involves several steps. First, assumptions are made to eliminate the nonlinearities that have negligible impact on the model accuracy. Second, we rearrange the elements in $\mathbf{x}$ to separate the linear and nonlinear terms of the system (11). Third, the KO theory is applied to eliminate the nonlinear terms by designing and extending tailored observable functions. The selection of appropriate observable functions is crucial to ensure the stabilizability of the new linear system for MG voltage control. Finally, we present the KO-linearized model in a concise form.

A. Assumptions

To simplify the derivation, we make some reasonable assumptions: 1) Since DER 1 is chosen as the common global reference, the difference angle between its global and local reference frame is $\delta_1 = 0$ with a zero initial value based on Eq. (7). Therefore, around the equilibrium, δ_i are small and we can approximate that $\sin \delta_i \approx \delta_i$ and $\cos \delta_i \approx 1$; 2) Since the $P - \omega$ droop gain is minuscule, we assume $\omega_i \approx \omega_n$ *only* in the coupling inductor terms in LC filters (5) and line currents (8). 3) More common resistive loads are considered in the following derivation to reduce the load dynamics. We rigorously test the model error caused by these assumptions in Section V-C under different conditions. The result shows that these assumptions are valid and acceptable.

B. Separating Linear and Nonlinear Subsystems

Based on the above assumptions, some state variables exhibit linear dynamics with respect to the system state $\mathbf{x}$ from Eq. (1) to Eq. (10). We simplify the derivation by directly extracting and incorporating these linear equations into the final KO-linearized model and addressing the remaining nonlinear dynamics with the KO.

1) Linear subsystems: Define state vector whose dynamics linearly depends on $\mathbf{x}$ as

$$\mathbf{x}_{\mathrm{L}i} = [\delta_i, \phi_{\mathrm{d}i}, \phi_{\mathrm{q}i}, \gamma_{\mathrm{d}i}, \gamma_{\mathrm{q}i}, i_{\mathrm{ld}i}, i_{\mathrm{lq}i}, v_{\mathrm{od}i}, v_{\mathrm{oq}i}]^\top, \quad i = 2, \ldots, m. \tag{13}$$

Since DER 1 is selected as the common reference, it has $\sin\delta_1 = 0$, $\cos\delta_1 = 1$ with $\delta_1(0) = 0$. Then, for DER 1, the nonlinearities caused by frame transformation (6) for $v_{\mathrm{bd}1}$ and $v_{\mathrm{bq}1}$ are eliminated, such that (5e)-(5f) become linear equations with $i = 1$, i.e.,

$$\mathbf{x}_{\mathrm{L}1} = [\phi_{\mathrm{d}1}, \phi_{\mathrm{q}1}, \gamma_{\mathrm{d}1}, \gamma_{\mathrm{q}1}, i_{\mathrm{ld}1}, i_{\mathrm{lq}1}, v_{\mathrm{od}1}, v_{\mathrm{oq}1}, i_{\mathrm{od}1}, i_{\mathrm{oq}1}]^\top. \tag{14}$$

The state-space model with respect to $\mathbf{x}_{\mathrm{L}} = [\mathbf{x}_{\mathrm{L}1}^\top, \ldots, \mathbf{x}_{\mathrm{L}m}^\top]^\top$ is derived respectively as

$$\dot{\mathbf{x}}_{\mathrm{L}1} = \mathcal{A}_{\mathrm{inv}1}\mathbf{x}_{\mathrm{L}1} + \mathcal{A}_1[Q_1, i_{\mathrm{lineD}1}, i_{\mathrm{lineQ}1}]^\top + \mathcal{B}_1 v_{\mathrm{set}1}, \tag{15}$$

$$\dot{\mathbf{x}}_{\mathrm{L}i} = \mathcal{A}_{\mathrm{inv}i}\mathbf{x}_{\mathrm{L}i} + \mathcal{A}_i[P_1, P_i, Q_i, i_{\mathrm{od}i}, i_{\mathrm{oq}i}]^\top + \mathcal{B}_i v_{\mathrm{set}i} \tag{16}$$

where $\mathcal{A}_{\mathrm{inv}1}$, $\mathcal{A}_{\mathrm{inv}i}$, $\mathcal{A}_1$ and $\mathcal{A}_i$ are given in (17)-(20), respectively and $\mathcal{B}_1 = [1, 0, K_{\mathrm{pv}1}, 0, b_1, 0, 0, 0, 0, 0]^\top$, $\mathcal{B}_i = [0, 1, 0, K_{\mathrm{pv}i}, 0, b_i, 0, 0, 0]^\top$ for $i = 2, \ldots, m$; moreover

$$a_{i,1} = \frac{K_{\mathrm{pc}i}K_{\mathrm{pv}i}D_{\mathrm{Q}i}}{L_{\mathrm{f}i}}, a_{i,2} = \frac{K_{\mathrm{pc}i}K_{\mathrm{iv}i}}{L_{\mathrm{f}i}}, a_{i,3} = \frac{K_{\mathrm{ic}i}}{L_{\mathrm{f}i}},$$
$$a_{i,4} = \frac{r_{\mathrm{f}i} + K_{\mathrm{pc}i}}{L_{\mathrm{f}i}}, a_{i,5} = \frac{1 + K_{\mathrm{pc}i}K_{\mathrm{pv}i}}{L_{\mathrm{f}i}}, a_{i,6} = \frac{K_{\mathrm{pc}i}\omega_{\mathrm{n}}C_{\mathrm{f}i}}{L_{\mathrm{f}i}},$$
$$a_{i,7} = \frac{K_{\mathrm{pc}i}F_i}{L_{\mathrm{f}i}}, a_{i,8} = \frac{r_{ci}}{L_{ci}} + \frac{R_{\mathrm{load}i}r_{\mathrm{n}}}{L_{ci}(r_{\mathrm{n}} + R_{\mathrm{load}i})},$$
$$a_{i,9} = \frac{R_{\mathrm{load}i}r_{\mathrm{n}}}{L_{ci}(r_{\mathrm{n}} + R_{\mathrm{load}i})}, b_i = \frac{K_{\mathrm{pc}i}K_{\mathrm{pv}i}}{L_{\mathrm{f}i}}, \text{ for } i = 1, \ldots, m.$$

$$\mathcal{A}_{\mathrm{inv}1} = \tag{17}$$
$$\begin{bmatrix}
0 & 0 & 0 & 0 & 0 & 0 & -1 & 0 & 0 & 0 \\
0 & 0 & 0 & 0 & 0 & 0 & 0 & -1 & 0 & 0 \\
K_{\mathrm{iv}1} & 0 & 0 & 0 & -1 & 0 & -K_{\mathrm{pv}1} & -\omega_{\mathrm{n}}C_{\mathrm{f}1} & F_1 & 0 \\
0 & K_{\mathrm{iv}1} & 0 & 0 & 0 & -1 & \omega_{\mathrm{n}}C_{\mathrm{f}1} & -K_{\mathrm{pv}1} & 0 & F_1 \\
a_{1,2} & 0 & a_{1,3} & 0 & -a_{1,4} & 0 & -a_{1,5} & -a_{1,6} & a_{1,7} & 0 \\
0 & a_{1,2} & 0 & a_{1,3} & 0 & -a_{1,4} & a_{1,6} & -a_{1,5} & 0 & a_{1,7} \\
0 & 0 & 0 & 0 & \frac{1}{C_{\mathrm{f}1}} & 0 & 0 & \omega_{\mathrm{n}} & -\frac{1}{C_{\mathrm{f}1}} & 0 \\
0 & 0 & 0 & 0 & 0 & \frac{1}{C_{\mathrm{f}1}} & -\omega_{\mathrm{n}} & 0 & 0 & -\frac{1}{C_{\mathrm{f}1}} \\
0 & 0 & 0 & 0 & 0 & 0 & \frac{1}{L_{\mathrm{c}1}} & 0 & -a_{1,8} & \omega_{\mathrm{n}} \\
0 & 0 & 0 & 0 & 0 & 0 & 0 & \frac{1}{L_{\mathrm{c}1}} & -\omega_{\mathrm{n}} & -a_{1,8}
\end{bmatrix}$$

$$\mathcal{A}_{\mathrm{inv}i} = \begin{bmatrix}
0 & 0 & 0 & 0 & 0 & 0 & 0 & 0 & 0 \\
0 & 0 & 0 & 0 & 0 & 0 & 0 & -1 & 0 \\
0 & 0 & 0 & 0 & 0 & 0 & 0 & 0 & -1 \\
0 & K_{\mathrm{iv}i} & 0 & 0 & 0 & -1 & 0 & -K_{\mathrm{pv}i} & -\omega_{\mathrm{n}}C_{\mathrm{f}i} \\
0 & 0 & K_{\mathrm{iv}i} & 0 & 0 & 0 & -1 & \omega_{\mathrm{n}}C_{\mathrm{f}i} & -K_{\mathrm{pv}i} \\
0 & a_{i,2} & 0 & a_{i,3} & 0 & -a_{i,4} & 0 & -a_{i,5} & -a_{i,6} \\
0 & 0 & a_{i,2} & 0 & a_{i,3} & 0 & -a_{i,4} & a_{i,6} & -a_{i,5} \\
0 & 0 & 0 & 0 & 0 & \frac{1}{C_{\mathrm{f}i}} & 0 & 0 & \omega_{\mathrm{n}} \\
0 & 0 & 0 & 0 & 0 & 0 & \frac{1}{C_{\mathrm{f}i}} & -\omega_{\mathrm{n}} & 0
\end{bmatrix} \tag{18}$$

$$\mathcal{A}_1 = \begin{bmatrix}
-D_{\mathrm{Q}1} & 0 & 0 \\
0 & 0 & 0 \\
-K_{\mathrm{pv}1}D_{\mathrm{Q}1} & 0 & 0 \\
0 & 0 & 0 \\
-a_{1,1} & 0 & 0 \\
0 & 0 & 0 \\
0 & 0 & 0 \\
0 & 0 & 0 \\
0 & a_{1,9} & 0 \\
0 & 0 & -a_{1,9}
\end{bmatrix} \tag{19}$$

$$\mathcal{A}_i = \begin{bmatrix}
D_{\mathrm{P}1} & -D_{\mathrm{P}i} & 0 & 0 & 0 \\
0 & 0 & -D_{\mathrm{Q}i} & 0 & 0 \\
0 & 0 & 0 & 0 & 0 \\
0 & 0 & -K_{\mathrm{pv}i}D_{\mathrm{Q}i} & F_i & 0 \\
0 & 0 & 0 & 0 & F_i \\
0 & 0 & -a_{i,1} & a_{i,7} & 0 \\
0 & 0 & 0 & 0 & a_{i,7} \\
0 & 0 & 0 & -\frac{1}{C_{\mathrm{f}i}} & 0 \\
0 & 0 & 0 & 0 & -\frac{1}{C_{\mathrm{f}i}}
\end{bmatrix} \tag{20}$$

2) Nonlinear subsystems (DER output power): We rewrite the dynamics of active and reactive powers (1) as

$$\underbrace{\begin{bmatrix}\dot{P}_i \\ \dot{Q}_i\end{bmatrix}}_{\dot{\mathbf{x}}_{\mathrm{pq}i}} = -\underbrace{\begin{bmatrix}\omega_{ci} & 0 \\ 0 & \omega_{ci}\end{bmatrix}}_{\mathbf{W}_{ci}}\underbrace{\begin{bmatrix}P_i \\ Q_i\end{bmatrix}}_{\mathbf{x}_{\mathrm{pq}i}} + \underbrace{\begin{bmatrix}\omega_{ci} & 0 \\ 0 & \omega_{ci}\end{bmatrix}}_{\mathbf{W}_{ci}}\underbrace{\begin{bmatrix}v_{\mathrm{od}i} & v_{\mathrm{oq}i} \\ v_{\mathrm{oq}i} & -v_{\mathrm{od}i}\end{bmatrix}}_{\mathbf{V}_{oi}}\underbrace{\begin{bmatrix}i_{\mathrm{od}i} \\ i_{\mathrm{oq}i}\end{bmatrix}}_{\mathbf{I}_{oi}} \triangleq \underbrace{\begin{bmatrix}z_{i,1} \\ z_{i,2}\end{bmatrix}}_{\mathbf{z}_{i,1}}. \tag{21}$$

In (21), $\mathbf{z}_{i,1}$ is a designed observable vector. For the control perspective, we take the second derivative of $\mathbf{z}_{i,1}$ until the control signal $\mathbf{u}$ appears in the second derivative of DER output voltage $\ddot{v}_{\mathrm{od}i}$. The derivation process is as follows,

$$\dot{\mathbf{z}}_{i,1} = -\mathbf{W}_{ci}\mathbf{z}_{i,1} + \mathbf{W}_{ci}(\dot{\mathbf{V}}_{oi}\mathbf{I}_{oi} + \dot{\mathbf{V}}_{oi}\dot{\mathbf{I}}_{oi}) \triangleq \mathbf{z}_{i,2}, \tag{22}$$

$$\dot{\mathbf{z}}_{i,2} = -\mathbf{W}_{ci}\mathbf{z}_{i,2} + \mathbf{W}_{ci}(\ddot{\mathbf{V}}_{oi}\mathbf{I}_{oi} + 2\dot{\mathbf{V}}_{oi}\dot{\mathbf{I}}_{oi} + \mathbf{V}_{oi}\ddot{\mathbf{I}}_{oi}). \tag{23}$$

Define the second term at the right-hand side of (23) as $\mathbf{U}_{\mathrm{pq}i}$:

$$\begin{aligned}\mathbf{U}_{\mathrm{pq}i} &= \mathbf{W}_{ci}(\ddot{\mathbf{V}}_{oi}\mathbf{I}_{oi} + 2\dot{\mathbf{V}}_{oi}\dot{\mathbf{I}}_{oi} + \mathbf{V}_{oi}\ddot{\mathbf{I}}_{oi}) \\ &= \mathbf{W}_{ci}\left(\begin{bmatrix}\ddot{v}_{\mathrm{oq}i}i_{\mathrm{oq}i}\end{bmatrix} + 2\dot{\mathbf{V}}_{oi}\dot{\mathbf{I}}_{oi} + \mathbf{V}_{oi}\ddot{\mathbf{I}}_{oi} + \begin{bmatrix}\ddot{v}_{\mathrm{od}i}i_{\mathrm{od}i} \\ -\ddot{v}_{\mathrm{od}i}i_{\mathrm{oq}i}\end{bmatrix}\right) \\ &\triangleq \mathbf{f}_{\mathrm{pq}i}(\mathbf{x}) + \mathcal{B}_{\mathrm{pq}i}\mathbf{u}\end{aligned} \tag{24}$$

where $\mathbf{f}_{\mathrm{pq}i}(\mathbf{x})$ is a nonlinear vector-valued function of $\mathbf{x}$ that can be extracted by substracting $\mathcal{B}_{\mathrm{pq}i}\mathbf{u}$ from $\mathbf{U}_{\mathrm{pq}i}$ and

$$\mathcal{B}_{\mathrm{pq}i} = \begin{bmatrix}\frac{b_i\omega_{ci}i_{\mathrm{od}i}}{C_{\mathrm{f}i}} & 0 & 0 \\ -\frac{b_i\omega_{ci}i_{\mathrm{oq}i}}{C_{\mathrm{f}i}} & 0 & 0\end{bmatrix}$$

In conclusion, we define the observable vector for the nonlinear subsystems with respect to DER output power as

$$\mathbf{z}_{\mathrm{pq}i} = \left[\mathbf{x}_{\mathrm{pq}i}^\top, \mathbf{z}_{i,1}^\top, \mathbf{z}_{i,2}^\top\right]^\top, \ i = 1, \ldots, m. \tag{25}$$

3) Nonlinear subsystems (currents of DERs and network): Since the DER output currents are coupled with the network currents, we handle them together and define

$$\mathbf{x}_{\text{net}} = [i_{\text{od}i}, i_{\text{oq}i}, i_{\text{line}\text{D}j}, i_{\text{line}\text{Q}j}]^\top, \quad i = 2, \ldots, m,\ j = 1, \ldots, q. \tag{26}$$

Then, from (5e)-(10), we rewrite the state equations as

$$\dot{\mathbf{x}}_{\text{net}} = \mathcal{A}_{\text{net}}\mathbf{x}_{\text{net}} + \mathbf{H}\xi + \mathbf{D}\mathbf{x}_{\text{net}} \triangleq \mathbf{z}_{\text{net}1}, \tag{27}$$

The positions of elements in $\mathcal{A}_{\text{net}}$, $\mathbf{H}$, and $\mathbf{D}$ depend on the topology of the MG. To illustrate the derivation, we take a test system shown in Fig. 3 as an example. Then, $\mathbf{x}_{\text{net}} = [i_{\text{od}2}, i_{\text{oq}2}, i_{\text{od}3}, i_{\text{oq}3}, i_{\text{lineD}1}, i_{\text{lineQ}1}, i_{\text{lineD}2}, i_{\text{lineQ}2}]^\top$, $\xi = [i_{\text{od}1}, i_{\text{oq}1}, v_{\text{od}2}, v_{\text{oq}2}, v_{\text{od}3}, v_{\text{oq}3}]^\top$ and the matrices are given as follows,

$$\mathcal{A}_{\text{net}} = \begin{bmatrix} -a_{2,8} & \omega_{\text{n}} & 0 & 0 & -a_{2,9} & 0 & a_{2,9} & 0 \\ -\omega_{\text{n}} & -a_{2,8} & 0 & 0 & 0 & a_{2,9} & 0 & -a_{2,9} \\ 0 & 0 & -a_{3,8} & \omega_{\text{n}} & 0 & 0 & -a_{3,9} & 0 \\ 0 & 0 & -\omega_{\text{n}} & -a_{3,8} & 0 & 0 & 0 & a_{3,9} \\ -\frac{r_{\text{n}}}{L_{\text{line}1}} & 0 & 0 & 0 & -a_{10} & \omega_{\text{n}} & \frac{r_{\text{n}}}{L_{\text{line}1}} & 0 \\ 0 & -\frac{r_{\text{n}}}{L_{\text{line}1}} & 0 & 0 & -\omega_{\text{n}} & -a_{10} & 0 & \frac{r_{\text{n}}}{L_{\text{line}1}} \\ \frac{r_{\text{n}}}{L_{\text{line}2}} & 0 & -a_{13} & 0 & \frac{r_{\text{n}}}{L_{\text{line}2}} & 0 & -a_{11} & \omega_{\text{n}} \\ 0 & \frac{r_{\text{n}}}{L_{\text{line}2}} & 0 & -a_{13} & 0 & \frac{r_{\text{n}}}{L_{\text{line}2}} & -\omega_{\text{n}} & -a_{11} \end{bmatrix} \tag{28}$$

$$\mathbf{H} = \begin{bmatrix} 0 & 0 & \frac{1}{L_{\text{c}2}} & 0 & 0 & 0 \\ 0 & 0 & 0 & \frac{1}{L_{\text{c}2}} & 0 & 0 \\ 0 & 0 & 0 & 0 & \frac{1}{L_{\text{c}3}} & 0 \\ 0 & 0 & 0 & 0 & 0 & \frac{1}{L_{\text{c}3}} \\ a_{12} & 0 & 0 & 0 & 0 & 0 \\ 0 & a_{12} & 0 & 0 & 0 & 0 \\ 0 & 0 & 0 & 0 & 0 & 0 \\ 0 & 0 & 0 & 0 & 0 & 0 \end{bmatrix} \tag{29}$$

$$\mathbf{D} = \begin{bmatrix} 0 & 0 & 0 & 0 & 0 & -a_{2,9}\delta_2 & 0 & a_{2,9}\delta_2 \\ 0 & 0 & 0 & 0 & a_{2,9}\delta_2 & 0 & -a_{2,9}\delta_2 & 0 \\ 0 & 0 & 0 & 0 & 0 & 0 & 0 & -a_{3,9}\delta_3 \\ 0 & 0 & 0 & 0 & 0 & 0 & a_{3,9}\delta_3 & 0 \\ 0 & \frac{r_{\text{n}}\delta_2}{L_{\text{line}1}} & 0 & 0 & 0 & 0 & 0 & 0 \\ \frac{-r_{\text{n}}\delta_2}{L_{\text{line}1}} & 0 & 0 & 0 & 0 & 0 & 0 & 0 \\ 0 & \frac{-r_{\text{n}}\delta_2}{L_{\text{line}2}} & 0 & a_{13}\delta_3 & 0 & 0 & 0 & 0 \\ \frac{r_{\text{n}}\delta_2}{L_{\text{line}2}} & 0 & -a_{13}\delta_3 & 0 & 0 & 0 & 0 & 0 \end{bmatrix} \tag{30}$$

where the parameters a_{10} to a_{13} are defined as

$$a_{10} = \frac{r_{\text{line}1} + r_{\text{n}}}{L_{\text{line}1}} + \frac{R_{\text{load}1} r_{\text{n}}}{L_{\text{line}1}(R_{\text{load}1} + r_{\text{n}})},$$
$$a_{11} = \frac{r_{\text{line}2} + r_{\text{n}}}{L_{\text{line}2}} + \frac{R_{\text{load}3} r_{\text{n}}}{L_{\text{line}2}(R_{\text{load}3} + r_{\text{n}})},$$
$$a_{12} = \frac{R_{\text{load}1} r_{\text{n}}}{L_{\text{line}1}(R_{\text{load}1} + r_{\text{n}})}, a_{13} = \frac{R_{\text{load}3} r_{\text{n}}}{L_{\text{line}2}(R_{\text{load}3} + r_{\text{n}})}$$

For the control purpose, we take the second derivative of $\mathbf{z}_{\text{net}1}$ until the control signal $\mathbf{u}$ appears in the second derivative of $\ddot{v}_{\text{od}i}$ in $\ddot{\xi}$. The derivation process is as follows,

$$\dot{\mathbf{z}}_{\text{net}1} = \mathcal{A}_{\text{net}}\mathbf{z}_{\text{net}1} + \mathbf{H}\dot{\xi} + \dot{\mathbf{D}}\mathbf{x}_{\text{net}} + \mathbf{D}\mathbf{z}_{\text{net}1} \triangleq \mathbf{z}_{\text{net}2}, \tag{31}$$

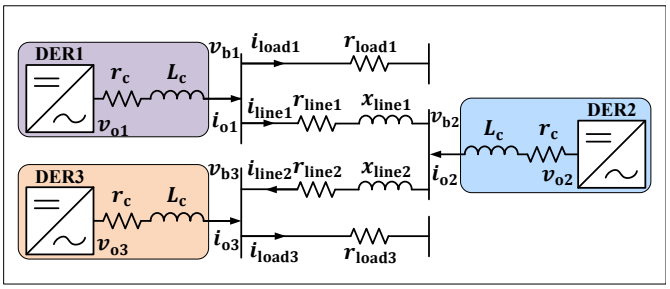

Fig. 3. Diagram of the test MG system.

$$\dot{\mathbf{z}}_{\text{net}2} = \mathcal{A}_{\text{net}}\mathbf{z}_{\text{net}2} + \ddot{\mathbf{D}}\mathbf{x}_{\text{net}} + 2\dot{\mathbf{D}}\mathbf{z}_{\text{net}1} + \mathbf{D}\mathbf{z}_{\text{net}2} + \mathbf{H}\ddot{\xi}. \tag{32}$$

Define the control vector $\mathbf{U}_{\text{net}}$ as (33). Note that $\mathbf{z}_{\text{net}1}$ and $\mathbf{z}_{\text{net}2}$ can be represented with $\mathbf{x}$, and $\mathbf{u}$ can be extracted from $\ddot{\xi}$, thus the control vector $\mathbf{U}_{\text{net}}$ can be separated as follows,

$$\begin{aligned} \mathbf{U}_{\text{net}} &= \ddot{\mathbf{D}}\mathbf{x}_{\text{net}} + 2\dot{\mathbf{D}}\mathbf{z}_{\text{net}1} + \mathbf{D}\mathbf{z}_{\text{net}2} + \mathbf{H}\ddot{\xi} \\ &= \underbrace{\ddot{\mathbf{D}}\mathbf{x}_{\text{net}} + 2\dot{\mathbf{D}}\mathbf{z}_{\text{net}1} + \mathbf{D}\mathbf{z}_{\text{net}2} + \mathbf{H}\ddot{\xi}^*}_{\mathbf{f}_{\text{net}}(\mathbf{x})} + \mathcal{B}_{\text{net}}\mathbf{u} \end{aligned} \tag{33}$$

where $\ddot{\xi}^* = \ddot{\xi} - \mathcal{B}_{\text{net}}\mathbf{u}$, $\mathcal{B}_{\text{net}} = \mathbf{H}\bar{\mathcal{B}}_{\text{net}}$ and

$$\bar{\mathcal{B}}_{\text{net}} = \begin{bmatrix} 0 & 0 & 0 \\ 0 & 0 & 0 \\ 0 & b_2 & 0 \\ 0 & 0 & 0 \\ 0 & 0 & b_3 \\ 0 & 0 & 0 \end{bmatrix} \tag{34}$$

In conclusion, we define the observable vector for the nonlinear subsystems with respect to DER output currents and the network as

$$\mathbf{z}_{\text{net}} = \left[\mathbf{x}_{\text{net}}^\top, \mathbf{z}_{\text{net}1}^\top, \mathbf{z}_{\text{net}2}^\top\right]^\top. \tag{35}$$

Remark 1: The treatment in the KO derivations (21)-(24) and (27)-(33) embodies a comparable concept to that of input-state feedback linearization. However, their intrinsic philosophies diverge significantly. Primarily, input-state feedback linearization endeavors to eliminate all nonlinearities in the state space by determining appropriate changes in state variables and employing feedback control laws. This process remains confined to the state space and typically does not result in an increase in state or input dimensions. Conversely, the proposed analytical method linearly represents the nonlinear MG system in a lifted observable space and control input space, which constitutes the fundamental characteristic of KO. Secondly, while input-state feedback can yield a perfectly linear model, achieving input-state feedback linearization necessitates meeting a series of feedback-linearizable conditions to guarantee the existence of a solution. These feedback-linearizable conditions (e.g., Theorem 13.2 in [30]) may not be applicable to MG and can be difficult to verify for high-order nonlinear systems. In contrast, the KO-based method can consistently furnish an approximated (or ideally, a perfect, contingent upon the impeccable selection of observables or infinite-dimensional considerations) linear model. Finally, due to the fundamentally distinct overall derivation philosophy, the final KO-linearized model (36) deviates from Brunovsky's canonical form as seen in feedback linearization.

C. Overall KO-linearized MG Model

Defining the observable vector of the overall MG system as $\mathbf{z} = \left[\mathbf{x}_{\mathrm{L}}^{\top}, \mathbf{z}_{\mathrm{pq1}}^{\top}, \ldots, \mathbf{z}_{\mathrm{pq}m}^{\top}, \mathbf{z}_{\mathrm{net}}^{\top}\right]^{\top} \in \mathbb{R}^{N}$, the KO-linearized model can be concluded as

$$\dot{\mathbf{z}} = \mathbf{A}\mathbf{z} + \mathbf{B}\mathbf{U}, \tag{36a}$$

$$\mathbf{y} = \mathbf{C}\mathbf{z} \tag{36b}$$

where $\mathbf{y} = [v_{\mathrm{od}1}, \ldots, v_{\mathrm{od}m}]^{\top} \in \mathbb{R}^{M}$ is the output vector, which can be extracted from the state vector with matrix $\mathbf{C}$, $\mathbf{U} = \left[\mathbf{u}^{\top}, \mathbf{U}_{\mathrm{pq1}}^{\top}, \ldots, \mathbf{U}_{\mathrm{pq}m}^{\top}, \mathbf{U}_{\mathrm{net}}^{\top}\right]$ is the lifted control input vector to be designed according to the control performance requirement. Take the system in Fig. 3 as an example, $m = 3$ and $N = 70$. Then the corresponding matrices $\mathbf{A}$ and $\mathbf{B}$ are derived as below

$$\mathbf{A} = \begin{bmatrix} \mathcal{A}_{\mathrm{inv}1} & \mathbf{0} & \mathbf{0} & \mathcal{A}_1^1 & \mathbf{0} & \mathbf{0} & \mathcal{A}_1^{2,3} & \mathbf{0} & \mathbf{0} \\ \mathbf{0} & \mathcal{A}_{\mathrm{inv}2} & \mathbf{0} & \mathcal{A}_2^1 & \mathcal{A}_2^{2,3} & \mathbf{0} & \mathcal{A}_2^{4,5} & \mathbf{0} & \mathbf{0} \\ \mathbf{0} & \mathbf{0} & \mathcal{A}_{\mathrm{inv}3} & \mathcal{A}_3^1 & \mathbf{0} & \mathcal{A}_3^{2,3} & \mathcal{A}_3^{4,5} & \mathbf{0} & \mathbf{0} \\ \mathbf{0} & \mathbf{0} & \mathbf{0} & \mathcal{A}_{\omega_1} & \mathbf{0} & \mathbf{0} & \mathbf{0} & \mathbf{0} & \mathbf{0} \\ \mathbf{0} & \mathbf{0} & \mathbf{0} & \mathbf{0} & \mathcal{A}_{\omega_2} & \mathbf{0} & \mathbf{0} & \mathbf{0} & \mathbf{0} \\ \mathbf{0} & \mathbf{0} & \mathbf{0} & \mathbf{0} & \mathbf{0} & \mathcal{A}_{\omega_3} & \mathbf{0} & \mathbf{0} & \mathbf{0} \\ \mathbf{0} & \mathbf{0} & \mathbf{0} & \mathbf{0} & \mathbf{0} & \mathbf{0} & \mathbf{0} & \mathbf{I}_8 & \mathbf{0} \\ \mathbf{0} & \mathbf{0} & \mathbf{0} & \mathbf{0} & \mathbf{0} & \mathbf{0} & \mathbf{0} & \mathbf{0} & \mathbf{I}_8 \\ \mathbf{0} & \mathbf{0} & \mathbf{0} & \mathbf{0} & \mathbf{0} & \mathbf{0} & \mathbf{0} & \mathbf{0} & \mathcal{A}_{\mathrm{net}} \end{bmatrix}_{70\times 70}$$

$$\mathbf{B} = \begin{bmatrix} \mathbf{B}_1 & \mathbf{B}_2 & \mathbf{B}_3 \end{bmatrix}_{70\times 17}$$

where the blocks regarding $\mathcal{A}_{\mathrm{inv}i}$ $(i = 1, \ldots, 3)$ at the upper-left of $\mathbf{A}$ correspond to the linear parts of the inverter models; the blocks regarding $\mathcal{A}_i^{j,k}$ at the upper-middle of $\mathbf{A}$ correspond to the linear part of DER output power and currents; the blocks regarding $\mathcal{A}_{\omega i}$ $(i = 1, \ldots, 3)$ at the middle of $\mathbf{A}$ correspond to the nonlinear part of DER output power and currents; the blocks regarding $\mathcal{A}_{\mathrm{net}}$ and $\mathbf{I}$ at the lower-right of $\mathbf{A}$ correspond to the network topology. $\mathbf{B}$ has a similar arrangement.

For simplification, we define the elements in $\mathbf{A}$ and $\mathbf{B}$ with MATLAB language (e.g., $\mathcal{A}_1(:, 2:3)$ means the second to the third columns of matrix $\mathcal{A}_1$ and ";" denotes line break) $\mathcal{A}_1^1 = [\mathbf{0}_{10\times 1}, \mathcal{A}_1(:,1), \mathbf{0}_{10\times 4}]$, $\mathcal{A}_1^{2,3} = [\mathbf{0}_{10\times 4}, \mathcal{A}_1(:, 2:3), \mathbf{0}_{10\times 2}]$, $\mathcal{A}_2^1 = [\mathcal{A}_2(:,1), \mathbf{0}_{9\times 5}]$, $\mathcal{A}_2^{2,3} = [\mathcal{A}_2(:, 2:3), \mathbf{0}_{9\times 4}]$, $\mathcal{A}_2^{4,5} = [\mathcal{A}_2(:, 4:5), \mathbf{0}_{9\times 6}]$, $\mathcal{A}_3^1 = [\mathcal{A}_3(:,1), \mathbf{0}_{9\times 5}]$, $\mathcal{A}_3^{2,3} = [\mathcal{A}_3(:, 2:3), \mathbf{0}_{9\times 4}]$, $\mathcal{A}_3^{4,5} = [\mathbf{0}_{9\times 2}, \mathcal{A}_3(:, 4:5), \mathbf{0}_{9\times 4}]$, $\mathbf{k}_i = [1, 0, K_{\mathrm{pv}i}0, b_i]^{\top}$ for $i = 1, 2, 3$. $\mathbf{B}_1 = [\mathbf{k}_1, \mathbf{0}_{1\times 65}; \mathbf{0}_{1\times 11}, \mathbf{k}_2, \mathbf{0}_{1\times 54}; \mathbf{0}_{1\times 20}, \mathbf{k}_3, \mathbf{0}_{1\times 45}]^{\top}$, $\mathbf{B}_2 = [\mathbf{0}_{2\times 32}, \mathbf{I}_2, \mathbf{0}_{2\times 36}; \mathbf{0}_{2\times 38}, \mathbf{I}_2, \mathbf{0}_{2\times 30}; \mathbf{0}_{2\times 44}, \mathbf{I}_2, \mathbf{0}_{2\times 24}]^{\top}$, $\mathbf{B}_3 = [\mathbf{0}_{62\times 8}; \mathbf{I}_8]$, and

$$\mathcal{A}_{\omega_i} = \begin{bmatrix} 0 & 0 & 1 & 0 & 0 & 0 \\ 0 & 0 & 0 & 1 & 0 & 0 \\ 0 & 0 & 0 & 0 & 1 & 0 \\ 0 & 0 & 0 & 0 & 0 & 1 \\ 0 & 0 & 0 & 0 & -\omega_{\mathrm{c}i} & 0 \\ 0 & 0 & 0 & 0 & 0 & -\omega_{\mathrm{c}i} \end{bmatrix}.$$

Remark 2: One of the benefits of model-based KO identification methods over data-driven ones is their scalability, which stems from the absence of data requirements. The proposed analytical KO identification methodology has a modular design that facilitates the scaling up of the MG. This can be achieved by simply inserting additional block matrices at the appropriate locations in the KO-linearized system matrices $\mathbf{A}$ and $\mathbf{B}$, and then adjusting the matrix $\mathcal{A}_{\mathrm{net}}$ to reflect the new network topology.

Remark 3: The purpose of the KO-linearized model (36) is to *enable general linear control techniques* that are still effective for the original nonlinear system. In practical application, the lifted-dimensional controller $\mathbf{U}$ will be designed based on the auxiliary linear model (36) using any general linear control methods. Then, an analytical actual control signal $\mathbf{u}$ will be obtained from $\mathbf{U}$. Finally, $\mathbf{u}$ will be applied to the original nonlinear MG system (11). It should also be noted that since part of system dynamics $\mathbf{F}(\mathbf{x})$ is included in the control term $\mathbf{B}\mathbf{U}$, one should not expect stability of the original nonlinear model (11) can be analyzed through the eigenvalues of $\mathbf{A}$ (assuming zero input) as usually done in small-signal models. This problem is further discussed in the case study section.

IV. Voltage Control of MG based on the KO-linearized Model

A critical contribution of this work is that users can select any linear control methods according to their requirements on their control objectives. In this section, we use MG's voltage restoration problem as an example to demonstrate how to use the above-developed linear MG model based on the KO theory. The control objective is to eliminate the steady-state errors between the output voltages of DERs and their reference values caused by the droop characteristics [2].

A. Controller Design based on KO-linearized Model with LQI

To achieve zero-offset voltage regulation and facilitate easy deployment, the optimal control method LQI is adopted in this section [17].

Firstly, as shown in the very left block in Fig. 4, an integrator that dynamically feeds back the integral of the offset between DER output voltages and their references is designed as follows,

$$\dot{\mathbf{z}}_{\mathrm{I}} = \mathbf{y}_{\mathrm{ref}} - \mathbf{y}, \tag{37}$$

where $\mathbf{z}_{\mathrm{I}}$ denotes the error dynamics of the integrator and $\mathbf{y}_{\mathrm{ref}}$ contains the voltage setpoints to be tracked.

Then, by defining new state vector $\tilde{\mathbf{z}} \triangleq \left[\mathbf{z}^{\top} - \mathbf{z}_{\infty}^{\top}, \mathbf{z}_{\mathrm{I}}^{\top}\right]^{\top}$, control input vector $\widetilde{\mathbf{U}} = [\mathbf{U} - \mathbf{U}_{\infty}]$ and output offset vector $\tilde{\mathbf{y}}(k) = \mathbf{y}(k) - \mathbf{y}_{\mathrm{ref}}$, the bias system is derived as follows,

$$\dot{\tilde{\mathbf{z}}} = \widetilde{\mathbf{A}}\tilde{\mathbf{z}} + \widetilde{\mathbf{B}}\widetilde{\mathbf{U}}, \tag{38a}$$

$$\tilde{\mathbf{y}} = \widetilde{\mathbf{C}}\tilde{\mathbf{z}} \tag{38b}$$

where the system matrices of the above-augmented system are given as

$$\widetilde{\mathbf{A}} = \begin{bmatrix} \mathbf{A} & \mathbf{0} \\ -\mathbf{C} & \mathbf{0} \end{bmatrix}, \widetilde{\mathbf{B}} = \begin{bmatrix} \mathbf{B} \\ \mathbf{0} \end{bmatrix}, \widetilde{\mathbf{C}} = \begin{bmatrix} \mathbf{C} & \mathbf{0} \end{bmatrix}. \tag{39}$$

Finally, to achieve offset-free setpoint tracking, the steady-state values $\mathbf{z}_{\infty}$ and $\mathbf{U}_{\infty}$ should satisfy

$$\begin{bmatrix} \mathbf{A} & \mathbf{B} \\ \mathbf{C} & \mathbf{0} \end{bmatrix} \begin{bmatrix} \mathbf{z}_{\infty} \\ \mathbf{U}_{\infty} \end{bmatrix} = \begin{bmatrix} \mathbf{0} \\ \mathbf{y}_{\mathrm{ref}} \end{bmatrix}. \tag{40}$$

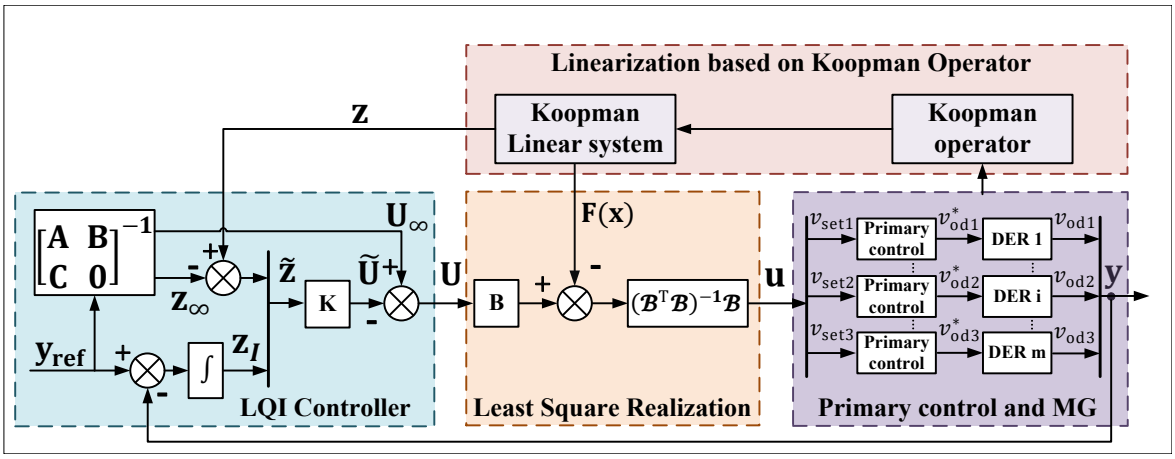

Fig. 4. Closed-loop MG control system based on the KO-linearized model and LQI. The LQI gain is $\mathbf{K} = \mathbf{R}^{-1}\widetilde{\mathbf{B}}^{\top}\mathbf{P}$.

Considering the following optimal performance index for the continuous-time system (38),

$$J = \frac{1}{2}\int_{t=0}^{\infty}(\tilde{\mathbf{z}}^{\top}\mathbf{Q}\tilde{\mathbf{z}} + \widetilde{\mathbf{U}}^{\top}\mathbf{R}\widetilde{\mathbf{U}})dt, \tag{41}$$

where $\mathbf{Q}$ and $\mathbf{R}$ are weighting matrices. The optimal control law minimizing J is derived as

$$\widetilde{\mathbf{U}} = -\mathbf{R}^{-1}\widetilde{\mathbf{B}}^{\top}\mathbf{P}\tilde{\mathbf{z}}, \tag{42}$$

$$\mathbf{U} = -\mathbf{R}^{-1}\widetilde{\mathbf{B}}^{\top}\mathbf{P}\tilde{\mathbf{z}} + \mathbf{U}_{\infty}, \tag{43}$$

where $\mathbf{P}$ is the unique positive definite solution to the following continuous-time algebraic Riccati equation

$$\widetilde{\mathbf{A}}^{\top}\mathbf{P} + \mathbf{P}\widetilde{\mathbf{A}} - \mathbf{P}\widetilde{\mathbf{B}}\mathbf{R}^{-1}\widetilde{\mathbf{B}}^{\top}\mathbf{P} + \mathbf{Q} = \mathbf{0}. \tag{44}$$

When the bias system (38)-(40) is stabilized by $\widetilde{\mathbf{U}}$ in Eq. (42), it is equivalent that: a) the KO-linearized model (36) is stabilized; b) the DER output voltages of (36), $\mathbf{y}$ is regulated to the setpoint $\mathbf{y}_{\text{ref}}$ with zero offsets, since $\dot{\mathbf{z}}_{\text{I}} = \mathbf{y}_{\text{ref}} - \mathbf{y} = 0$.

B. Recovering Lower-Dimensional Control Signal for the Original MG System from the Lifted Control Vector

Note that the lifted control vector $\mathbf{U} \in \mathbb{R}^{M}$ of the KO-linearized model (36) is of higher dimensional than the control vector $\mathbf{u} \in \mathbb{R}^{m}$ of the original nonlinear MG model (11). Thus, the lifted control signal $\mathbf{U}$ is not directly applicable. Since the first three elements of $\mathbf{U}$ are just $\mathbf{u}$, one can use them as the control inputs of the original MG system. However, such a choice is no longer optimal due to the loss of information of the other elements in $\mathbf{U}$. Therefore, we propose the following optimal control signal recovery method.

Denote $\mathbf{U}_{\text{pq}} = [\mathbf{U}_{\text{pq}1}, \ldots, \mathbf{U}_{\text{pq}m}]^{\top}$, $\mathcal{B}_{\text{pq}} = [\mathcal{B}_{\text{pq}1}, \ldots, \mathcal{B}_{\text{pq}m}]^{\top}$ and $\mathbf{f}_{\text{pq}} = [\mathbf{f}_{\text{pq}1}, \ldots, \mathbf{f}_{\text{pq}m}]^{\top}$, from (24) and (33), it has

$$\begin{aligned}\mathbf{BU} &= \mathbf{B}_1\mathbf{u} + \mathbf{B}_2\mathbf{U}_{\text{pq}} + \mathbf{B}_3\mathbf{U}_{\text{net}} \\ &= \mathbf{B}_1\mathbf{u} + \mathbf{B}_2\left(\mathbf{f}_{\text{pq}}(\mathbf{x}) + \mathcal{B}_{\text{pq}}\mathbf{u}\right) + \mathbf{B}_3\left(\mathbf{f}_{\text{net}}(\mathbf{x}) + \mathcal{B}_{\text{net}}\mathbf{u}\right) \\ &= \underbrace{\mathbf{B}_2\mathbf{f}_{\text{pq}}(\mathbf{x}) + \mathbf{B}_3\mathbf{f}_{\text{net}}(\mathbf{x})}_{\mathbf{F}(\mathbf{x})} + \underbrace{\left(\mathbf{B}_1 + \mathbf{B}_2\mathcal{B}_{\text{pq}} + \mathbf{B}_3\mathcal{B}_{\text{net}}\right)}_{\mathcal{B}}\mathbf{u}\end{aligned} \tag{45}$$

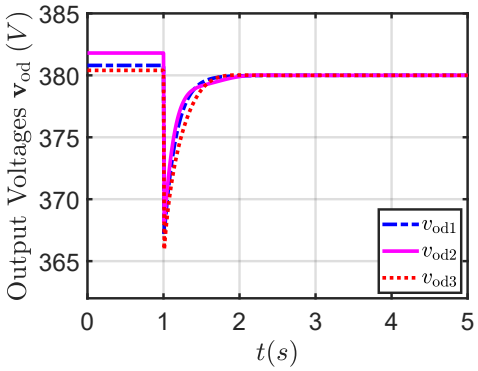

Fig. 5. Dynamic responses of DER output voltages of the test MG.

Notice that matrix $\mathcal{B}$ is not a square matrix such that $\mathbf{u}$ cannot be directly retrieved via $\mathcal{B}^{-1}$. Therefore, we optimally recover $\mathbf{u}$ from $\mathbf{U}$ by solving the following least square problem,

$$\min \frac{1}{2}\left(\mathcal{B}\mathbf{u} - (\mathbf{BU} - \mathbf{F}(\mathbf{x}))\right)^{\top}\left(\mathcal{B}\mathbf{u} - (\mathbf{BU} - \mathbf{F}(\mathbf{x}))\right) \tag{46}$$

whose solution is

$$\mathbf{u} = (\mathcal{B}^{\top}\mathcal{B})^{-1}\mathcal{B}^{\top}\left(\mathbf{BU} - \mathbf{F}(\mathbf{x})\right). \tag{47}$$

By substituting (43) into (47), the controller for original MG (11) is obtained as follows

$$\mathbf{u} = (\mathcal{B}^{\top}\mathcal{B})^{-1}\mathcal{B}^{\top}\left(\mathbf{BU}_{\infty} - \mathbf{BR}^{-1}\widetilde{\mathbf{B}}^{\top}\mathbf{P}\tilde{\mathbf{z}} - \mathbf{F}(\mathbf{x})\right) \tag{48}$$

Remark 4: The nonlinear term $\mathbf{F}(\mathbf{x})$ in the control law (48) has a known expression that can be computed by inserting the values of the state variables $\mathbf{x}$. Moreover, $\mathbf{U}_{\infty}$ and $\mathbf{z}_{\infty}$ are calculated through Eq. (40), $\mathbf{z}$ in $\tilde{\mathbf{z}}$ can be substituted by the designed measurement function $\mathbf{z} = \mathbf{g}(\mathbf{x}, \mathbf{u})$ and $\mathbf{z}_{\text{I}}$ can be directly obtained via the integrator (37). Thus, the controller (48) only requires feedback of $\mathbf{x}$ and is ready to be implemented in the original MG system (11).

The overall closed-loop MG control system based on the KO and LQI is shown in Fig. 4.

V. Case Studies

This section presents several case studies that demonstrate the effectiveness of using the developed KO-linearized model

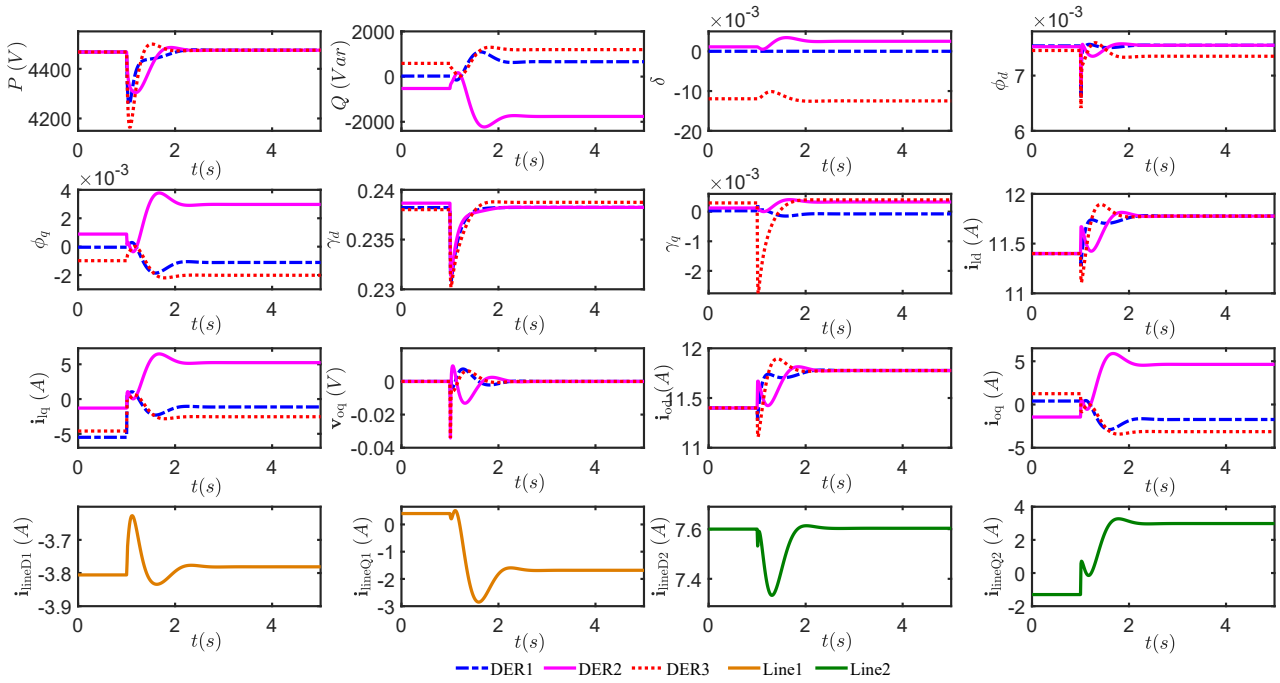

Fig. 6. Dynamic responses of all the other state variables of the test MG.

TABLE I
PARAMETER SETTING OF MG

	Par.	Value	Par.	Value
Initial	$\mathbf{v}_{\mathrm{od}}(0)$	$[380.8, 381.8, 380.4]$	$\mathbf{v}_{\mathrm{oq}}(0)$	$[0, 0, 0]$
	$\mathbf{i}_{\mathrm{od}}(0)$	$[11.4, 11.4, 11.4]$	$\mathbf{i}_{\mathrm{oq}}(0)$	$[0.4, -1.45, 1.25]$
	$\mathbf{i}_{\mathrm{ld}}(0)$	$[11.4, 11.4, 11.4]$	$\mathbf{i}_{\mathrm{lq}}(0)$	$[-5.5, -7.3, -4.6]$
	$\omega(0)$	314	$\boldsymbol{\delta}_0$	$[0, 0.0019, -0.0113]$
	$i_{\mathrm{line1d}}(0)$	-3.8	$i_{\mathrm{line1q}}(0)$	0.4
	$i_{\mathrm{line2d}}(0)$	7.6	$i_{\mathrm{line2q}}(0)$	-1.3
Line and Load	r_{line1}	0.23 Ω	x_{line1}	0.1 Ω
	r_{line2}	0.35 Ω	x_{line2}	0.58 Ω
	r_{load1}	25 Ω	x_{load3}	20 Ω
DER	The DER parameters can be found in [8]			

with the traditional LQI control method to stabilize the original nonlinear MG system and eliminate the steady-state error of DER output voltages caused by the droop equations.

A. Simulation Setup

The test system is a widely used 220 V MG with three inverter-based DERs as shown in Fig. 3 [8]. The network is resistance-dominated for such a low-voltage distribution system. Table I provides the parameter setting and initial states in this section. All three DERs are rated at 10 kVA with the same droop gain, so the load consumption is shared equally. Before the designed controller $\mathbf{u}$ in (48) is applied, the voltage setpoints $v_{\mathrm{set}i}$ $(i = 1, \ldots, 3)$ in the droop equation (2b) for each DER are set as 380 V, resulting in steady-state errors in DER output voltages $v_{\mathrm{od}i}$. All the dynamic simulations are conducted in the MATLAB environment on a standard PC with an Intel(R) Core(TM) i9-13900HX CPU running at 2.20 GHz and with 32.0 GB of RAM.

B. Control Performance based on the KO and LQI

The proposed KO-linearized MG model for the voltage control of MGs is verified by applying the LQI controller (48) to the original nonlinear MG model (11) after 1 s. Before that, the voltage setpoints for the droop equations are kept constant at $\mathbf{u} = [380, 380, 380]^\top$ V. Figure 5 shows that the DER output voltages have steady-state errors due to the droop characteristic before 1 s. When the proposed KO-based LQI controller takes over, the steady-state errors are quickly eliminated, confirming the effectiveness of the proposed method.

Figure 6 shows the dynamic responses of all the other stable variables. It can be observed that all the state variables are stabilized to a new equilibrium point. For a more systematic study of the system stability, we compare the poles of the system (36) before and after the LQI controller $\widetilde{\mathbf{U}}$ are applied, i.e., eigenvalues of $\mathbf{A}$ and $\widetilde{\mathbf{A}} - \widetilde{\mathbf{B}}\widetilde{\mathbf{K}}$. The maximum of the real part of eigenvalues of matrix $\mathbf{A}$ is 7.7709×10^{-11} while that of matrix $\widetilde{\mathbf{A}} - \widetilde{\mathbf{B}}\widetilde{\mathbf{K}}$ is -9.4000×10^{-4}. However, it should be mentioned that the original nonlinear system (11) is actually stable with the provided configuration. The reason that the KO-linearized model (36) has positive poles (indicating unstable modes) is that part of system dynamics $\mathbf{F}(\mathbf{x})$ is absorbed into the term $\mathbf{BU}$ as discussed in Remark 1. Therefore, the poles of $\mathbf{A}$ only reflect the open-loop stability of the KO-linearized system (36), but do not indicate the stability of the original nonlinear system (11). With the application of LQI, all the poles are placed on the plane's left side, indicating that the LQI controller stabilizes the system (36) as shown in Fig. 7.

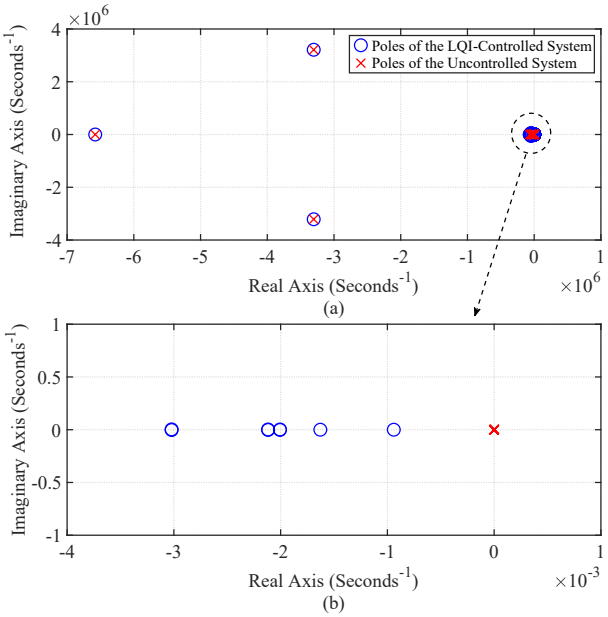

Fig. 7. Comparison of poles of system (36) before and after the LQI controller $\tilde{\mathbf{U}}$ is applied.

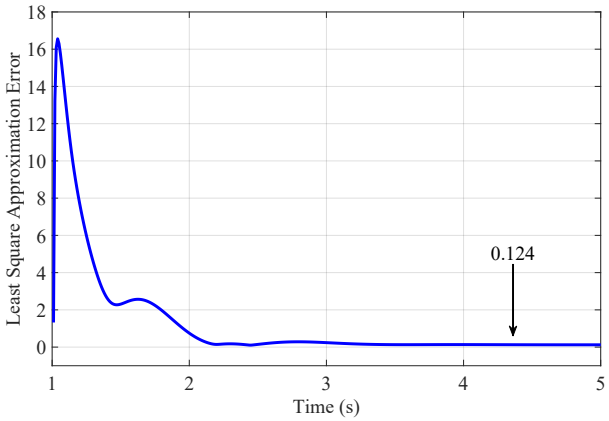

Fig. 8. The time-varying approximation error of the control signal using the least square method (46).

The lifted control vector $\mathbf{U}$ can stabilize the MG system as verified by the above pole analysis. However, the proposed KO-based control scheme also relies on the approximation of the original control input $\mathbf{u}$ by solving the least square optimization problem (46), which introduces an approximation error. Figure 8 shows that the least square approximation error converges to a small value of 0.124 after 4 s, implying that the approximation error has a negligible impact on the overall control performance in this case.

C. Model Error and Sensitivity Analyses

The KO-linearized model (36) is derived analytically, so the only source of model error between (36) and (11) should be the assumptions made in the model development, namely $\sin\delta_i \approx \delta_i$, $\cos\delta_i \approx 1$, and $\omega_i \approx \omega_n$ in the LC filters and lines. To verify this claim, we set $\mathbf{u} = [380, 380, 380]^\top$ V for both (11) and (36). Since the observable vector $\mathbf{z}$ contains an explicit representation of the state vector of the original MG $\mathbf{x}$, we can denote the $\mathbf{x}$ in $\mathbf{z}$ as $\mathbf{z}_\mathbf{x}$. This allows us to directly compare the dynamic responses of the two models. Use mean absolute error (MAE) to define the model error as

$$\mathrm{MAE}(t) = \frac{1}{n}\sum_{i=1}^{n} |\mathbf{x}(t) - \mathbf{z}_\mathbf{x}(t)|\,. \tag{49}$$

We also conduct sensitivity analysis of the developed KO-linearized model by simulating 50 different sets of initial conditions. For each run, we add a 30% random perturbation to the initial condition in Table I. Figure 9 shows that all the model errors $\mathrm{MAE}(t)$ with different initial conditions oscillate during the settling period and finally converge to around 0.357. Moreover, the $\mathrm{MAE}(t)$ is always below 1 throughout the timeline. To investigate the source of the steady-state error, we examine the detailed error of each state. Figure 10 reveals that the steady-state errors mainly occur in the active and reactive powers, but their actual values are negligible compared to the magnitude of P and Q. Therefore, we conclude that the developed KO-linearized model is sufficiently accurate and robust against different initial conditions.

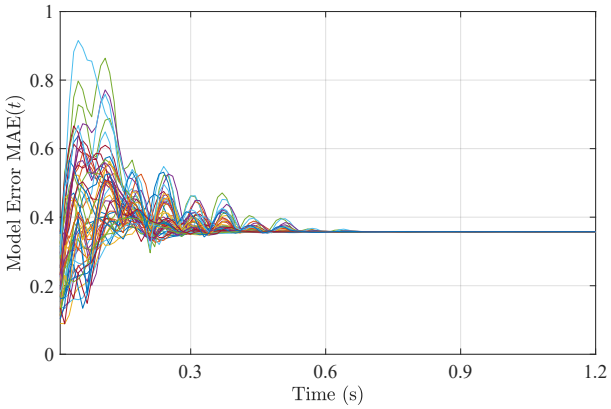

Fig. 9. The time-varying model error measured by MAE with 50 different initial condition settings.

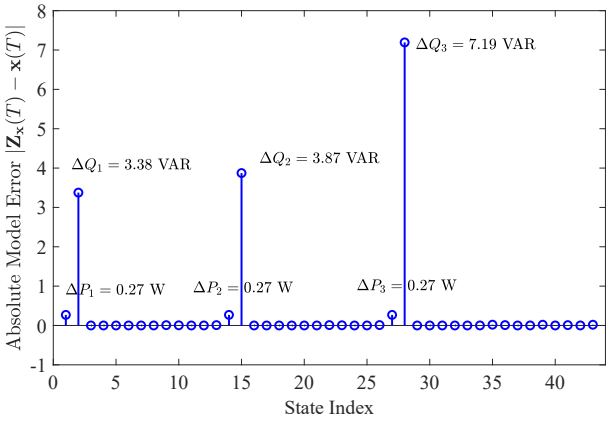

Fig. 10. The steady-state absolute model error of each state at time $T = 5$ seconds. ΔP and ΔQ denote the absolute error of real and reactive powers, respectively.

D. Comparison Case Studies

This subsection compares the proposed LQI control method

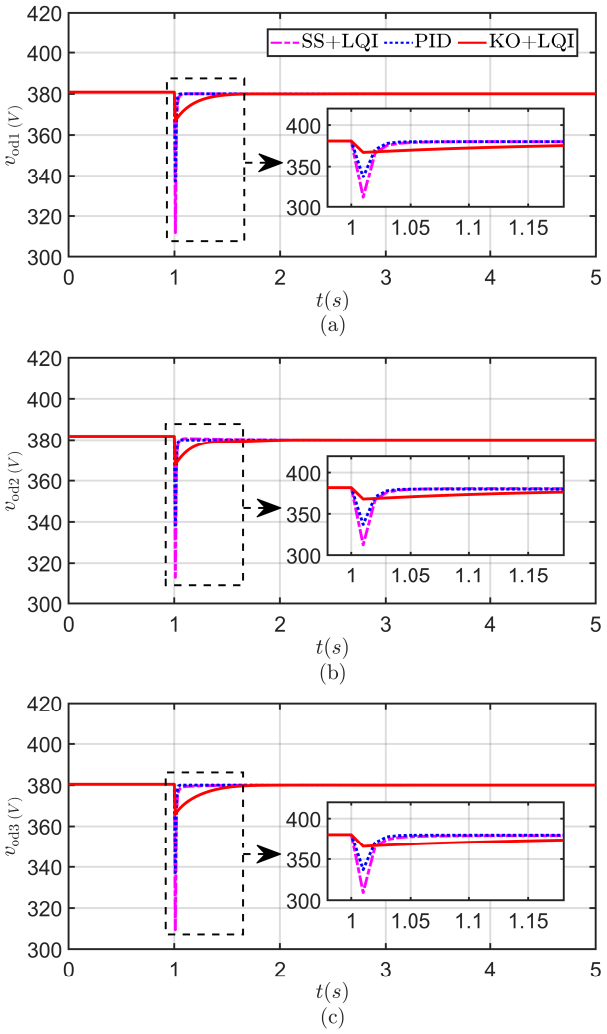

Fig. 11. Comparison of the control performances of DER output voltages using the small-signal-model-based LQI (SS+LQI), original-nonlinear-model-based PID, and the proposed KO-linearized-model-based LQI (KO+LQI).

based on the KO-linearized model with two common MG voltage control methods. The first method is a proportional-integral-derivative (PID) control based on the original nonlinear MG model (11), with the output function $\mathbf{y} = [v_{od1}, v_{od2}, v_{od3}]$. The proportional, integral, and derivative gains for all three PID controllers are set to 1.5, 320, and 0, respectively. The second method is an LQI control based on the small-signal model (first-order Taylor expansion) from [8], with the same LQI setting as in Section V-B.

As shown in Fig. 11, the PID and SS+LQI achieve significantly faster dynamic response speeds than the KO+LQI. However, they also lead to much larger overshoots during the transients, which are hazardous for MG operation. Furthermore, the comparison between SS+LQI and KO+LQI reveals that the proposed KO-linearized model can capture the nonlinear dynamics more precisely than the small-signal model based on first-order Taylor expansion, resulting in a smoother dynamic performance.

E. Computational Efficiency Analysis

The performance of the KO-based method in terms of computational efficiency can be evaluated by considering two aspects: the identification of KO and the dynamic simulation of the controlled MG system.

Firstly, the proposed KO identification method is fully model-based which means the analytical linear system (36) is manually derived offline. Therefore, the proposed analytical KO derivation approach does not require any computational effort. This contrasts with the data-driven methods that rely on numerical computation of the KO [20]–[26].

The second aspect of the computational efficiency of the KO-based method is the impact of the increased dimension of the studied MG system, which is lifted from 43 to 70 in this case. To assess this impact, we compare the computational times of dynamic simulations of the proposed KO+LQI method with the two other methods (based on unlifted-dimensional MG models) studied in Section V-D. The simulation is performed using the ode15s solver with 0.01 s sampling time over 5 s dynamic simulation duration in MATLAB. The average computational times over 100 runs of PID, SS+LQI, and the proposed KO+LQI methods are 0.0218 s, 0.0232 s, and 0.0422 s, respectively. We can see that, the computational times of PID and SS+LQI are similar because they both use the original 43-dimensional MG system. On the other hand, the computational time of the proposed KO+LQI method is higher than the others mainly due to the increased system dimension, however, it is still sufficiently fast for practical implementation.

VI. Conclusions

This paper presents a novel large-signal method to linearize microgrid (MG) models for controller design using the Koopman operator (KO) theory. The primary and zero control levels are modeled for electromagnetic transient (EMT) analysis, which increases system order and nonlinearity. To overcome these challenges, we have derived the observable functions and KO analytically, avoiding data dependence and improving explainability. Voltage control with linear quadratic integrator (LQI) is used as an example to show how our KO-linearized model enables textbook linear control techniques for nonlinear MGs. To guarantee stabilizability, a lifted-dimensional control signal has been derived in the KO-linearized model. We use least squares to map the high-dimensional control vector to the original one. The case studies validate the LQI and KO-linearized model for DER output voltage restoration. The model error without a state-feedback controller under different initial conditions confirms the accuracy and robustness of our analytical KO-linearized MG model. Comparison case studies with benchmark approaches such as PID and small-signal-model-based methods are conducted to validate the advantages of the proposed KO-based MG voltage control scheme. The proposed analytical derivation methodology is generic and applicable to other MG systems with different structures and objectives due to a modular design.

Our future work will focus on discovering the theoretical stability analysis of the original nonlinear system (11), i.e.,

developing a sufficient condition with respect to $\mathbf{A}, \mathbf{B}, \mathbf{F}(\mathbf{x})$ and $\mathcal{B}$, under which, the control signal $\mathbf{u}$ recovered by the least square method can *theoretically* ensure the stability of the original system (11). This mathematical problem is still fundamentally challenging, but its solution can contribute to addressing a wide class of nonlinear control problems.

REFERENCES

[1] J. C. Vasquez, J. M. Guerrero, J. Miret, M. Castilla, and L. G. de Vicuña, "Hierarchical control of intelligent microgrids," *IEEE Ind. Electron. Mag*, vol. 4, no. 4, pp. 23–29, Dec. 2010.

[2] A. Bidram and A. Davoudi, "Hierarchical structure of microgrids control system," *IEEE Trans. Smart Grid*, vol. 3, no. 4, pp. 1963–1976, Dec. 2012.

[3] Q. Zhang, Z. Ma, Y. Zhu, and Z. Wang, "A two-level simulation-assisted sequential distribution system restoration model with frequency dynamics constraints," *IEEE Trans. Smart Grid*, vol. 12, no. 5, pp. 3835–3846, Sept. 2021.

[4] Z. Ma, Z. Wang, Y. Guo, Y. Yuan, and H. Chen, "Nonlinear multiple models adaptive secondary voltage control of microgrids," *IEEE Trans. Smart Grid*, vol. 12, no. 1, pp. 227–238, Jan. 2021.

[5] R. Cheng, N. Shi, S. Maharjan, and Z. Wang, "Automatic self-adaptive local voltage control under limited reactive power," *IEEE Trans. Smart Grid*, vol. 14, no. 4, pp. 2851–2862, Nov. 2023.

[6] B. Chen, J. Wang, X. Lu, C. Chen, and S. Zhao, "Networked microgrids for grid resilience, robustness, and efficiency: A review," *IEEE Trans. Smart Grid*, vol. 12, no. 1, pp. 18–32, 2021.

[7] W. Cui, Y. Jiang, and B. Zhang, "Reinforcement learning for optimal primary frequency control: A lyapunov approach," *IEEE Trans. Power Syst.*, vol. 38, no. 2, pp. 1676–1688, Mar. 2023.

[8] N. Pogaku, M. Prodanovic, and T. C. Green, "Modeling, analysis and testing of autonomous operation of an inverter-based microgrid," *IEEE Trans. Power Electron.*, vol. 22, no. 2, pp. 613–625, Mar. 2007.

[9] M. Rasheduzzaman, J. A. Mueller, and J. W. Kimball, "An accurate small-signal model of inverter- dominated islanded microgrids using *dq* reference frame," *IEEE J. Emerg. Sel. Top. Power Electron.*, vol. 2, no. 4, pp. 1070–1080, Dec. 2014.

[10] Q. Shafiee, Č. Stefanović, T. Dragičević, P. Popovski, J. C. Vasquez, and J. M. Guerrero, "Robust networked control scheme for distributed secondary control of islanded microgrids," *IEEE Trans. Ind. Electron.*, vol. 61, no. 10, pp. 5363–5374, Oct. 2014.

[11] A. Bidram, A. Davoudi, F. L. Lewis, and J. M. Guerrero, "Distributed cooperative secondary control of microgrids using feedback linearization," *IEEE Trans. Power Syst.*, vol. 28, no. 3, pp. 3462–3470, Aug. 2013.

[12] A. Bidram, F. L. Lewis, and A. Davoudi, "Distributed control systems for small-scale power networks: Using multiagent cooperative control theory," *IEEE Control Syst. Mag.*, vol. 34, no. 6, pp. 56–77, Dec. 2014.

[13] Y. Du, X. Lu, B. Chen, and F. Lin, "Resiliency augmented hybrid AC and DC distribution systems with inverter-dominated dynamic microgrids," *IEEE Trans. Smart Grid*, vol. 13, no. 5, pp. 4088–4101, Sept. 2022.

[14] J. Lai, X. Lu, and X. Yu, "Stochastic distributed frequency and load sharing control for microgrids with communication delays," *IEEE Syst. J*, vol. 13, no. 4, pp. 4269–4280, Dec. 2019.

[15] J. Lai, X. Lu, X. Yu, and A. Monti, "Stochastic distributed secondary control for ac microgrids via event-triggered communication," *IEEE Trans. Smart Grid*, vol. 11, no. 4, pp. 2746–2759, Jul. 2020.

[16] A. Maulik and D. Das, "Stability constrained economic operation of islanded droop-controlled dc microgrids," *IEEE Trans. Sustain. Energy*, vol. 10, no. 2, pp. 569–578, Apr. 2019.

[17] Z. Ma, Q. Zhang, and Z. Wang, "Safe and stable secondary voltage control of microgrids based on explicit neural networks," *IEEE Trans. Smart Grid*, 2023, early access. doi=10.1109/TSG.2023.3239548.

[18] B. O. Koopman, "Hamiltonian systems and transformation in hilbert space," *Proceedings of the National Academy of Sciences*, vol. 17, no. 5, pp. 315–318, Mar. 1931.

[19] J. Yao, Q. Hu, and J. Zheng, "Koopman-operator-based safe learning control for spacecraft attitude reorientation with angular velocity constraints," *IEEE Trans. Aerosp. Electron. Syst.*, pp. 1–14, 2023, early access. doi=10.1109/TAES.2023.3285725.

[20] A. E. Saldaña, E. Barocio, A. R. Messina, J. J. Ramos, R. J. Segundo, and G. A. Tinajero, "Monitoring harmonic distortion in microgrids using dynamic mode decomposition," in *2017 IEEE Power & Energy Society General Meeting*, 2017, pp. 1–5.

[21] G. Kandaperumal, K. P. Schneider, and A. K. Srivastava, "A data-driven algorithm for enabling delay tolerance in resilient microgrid controls using dynamic mode decomposition," *IEEE Trans. Smart Grid*, vol. 13, no. 4, pp. 2500–2510, Jul. 2022.

[22] M. O. Williams, I. G. Kevrekidis, and C. W. Rowley, "A data-driven approximation of the Koopman operator: Extending dynamic mode decomposition," *J. Nonlinear Sci.*, vol. 25, pp. 1307–1346, Jun. 2015.

[23] M. Korda and I. Mezić, "Linear predictors for nonlinear dynamical systems: Koopman operator meets model predictive control," *Automatica*, vol. 93, pp. 149–160, Jul. 2018.

[24] V. Toro, D. Tellez-Castro, E. Mojica-Nava, and N. Rakoto-Ravalontsalama, "Data-driven distributed voltage control for microgrids: A koopman-based approach," *Int. J. Electr. Power Energy Syst.*, vol. 145, p. 108636, Feb. 2023.

[25] X. Gong, X. Wang, and G. Joos, "An online data-driven method for microgrid secondary voltage and frequency control with ensemble Koopman modeling," *IEEE Trans. Smart Grid*, vol. 14, no. 1, pp. 68–81, Jan. 2023.

[26] X. Gong and X. Wang, "A novel Koopman-inspired method for the secondary control of microgrids with grid-forming and grid-following sources," *Appl. Energy*, vol. 333, p. 120631, Mar. 2023.

[27] S. Servadio, D. Arnas, and R. Linares, "Dynamics near the three-body libration points via Koopman operator theory," *J. Guid. Control Dyn.*, vol. 45, no. 10, pp. 1800–1814, Jul. 2022.

[28] T. Chen and J. Shan, "Koopman-operator-based attitude dynamics and control on SO(3)," *J. Guid. Control Dyn.*, vol. 43, no. 11, p. 2112–2126, Nov. 2020.

[29] D. Arnas and R. Linares, "Approximate analytical solution to the zonal harmonics problem using Koopman operator theory," *J. Guid. Control Dyn.*, vol. 44, no. 11, pp. 1909–1923, Aug. 2021.

[30] H. K. Khalil, *Nonlinear Systems*. New Jersey: Prentice Hall, 2000.

Zixiao Ma (Member, IEEE) received his B.S. degree in automation and M.S. degree in control theory and control engineering from Northeastern University, Shenyang, China, in 2014 and 2017, respectively, and the Ph.D. degree in electrical and computer engineering from Iowa State University, Ames, IA, USA, in 2023. He is currently a Postdoctoral Scholar in the Clean Energy Institute and Department of Electrical and Computer Engineering at the University of Washington, Seattle, WA, USA. He was the recipient of the Outstanding Reviewer Award from IEEE Transactions on Power Systems, the Research Excellence Award from Iowa State University, the Chinese Government Award for Outstanding Self-financed Students Abroad, and the Distinguished Postdoctoral Fellowship from the University of Washington. His research interests focus on control theory and machine learning with their applications to inverter-based resources, microgrids, and load modeling.

Zhaoyu Wang (Senior Member, IEEE) received the B.S. and M.S. degrees in electrical engineering from Shanghai Jiao Tong University, and the M.S. and Ph.D. degrees in electrical and computer engineering from Georgia Institute of Technology. He is the Northrop Grumman Endowed Associate Professor with Iowa State University. His research interests include optimization and data analytics in power distribution systems and microgrids. He was the recipient of the National Science Foundation CAREER Award, the Society-Level Outstanding Young Engineer Award from IEEE Power and Energy Society (PES), the Northrop Grumman Endowment, College of Engineering's Early Achievement in Research Award, and the Harpole-Pentair Young Faculty Award Endowment. He is the Principal Investigator for a multitude of projects funded by the National Science Foundation, the Department of Energy, National Laboratories, PSERC, and Iowa Economic Development Authority. He is the Technical Committee Program Chair (TCPC) of IEEE Power System Operation, Planning and Economics (PSOPE) Committee, the Chair of IEEE PSOPE Award Subcommittee, the Vice Chair of IEEE Distribution System Operation and Planning Subcommittee, and the Vice Chair of IEEE Task Force on Advances in Natural Disaster Mitigation Methods. He is an Associate Editor of IEEE TRANSACTIONS ON SUSTAINABLE ENERGY, IEEE OPEN ACCESS JOURNAL OF POWER AND ENERGY, IEEE POWER ENGINEERING LETTERS, and IET Smart Grid. He was an Associate Editor for IEEE TRANSACTIONS ON POWER SYSTEMS and IEEE TRANSACTIONS ON SMART GRID.

Rui Cheng (Member, IEEE) is currently the Assistant Professor at North China Electric Power University. He received the Ph.D. degree in electrical engineering from Iowa State University in 2023. He was the recipient of the Best Paper Award from the 2023 IEEE Power & Energy Society General Meeting, and the Research Excellence Award from Iowa State University. His research interests include power distribution systems, voltage/var control, transactive energy markets, power system reliability and resilience, and applications of optimization and machine learning methods to power systems.